Geophys. J. Int. (1996) **126,** 235–252

Approximate sensitivities for the electromagnetic inverse problem

C. G. Farquharson and D. W. Oldenburg

UBC–Geophysical Inversion Facility, Department of Earth and Ocean Sciences, Geophysics Building, 2219 Main Mall, University of British Columbia, Vancouver, BC, V6T 1Z4, Canada

Accepted 1996 March 18. Received 1996 March 13; in original form 1995 July 10

SUMMARY

We present an approximate method for generating the Jacobian matrix of sensitivities required by linearized, iterative procedures for inverting electromagnetic measurements. The approximation is based on the adjoint-equation method in which the sensitivities are obtained by integrating, over each cell, the scalar product of an adjoint electric field (the adjoint Green's function) with the electric field produced by the forward modelling at the end of the preceding iteration. Instead of computing the adjoint field in the multidimensional conductivity model, we compute an approximate adjoint field, either in a homogeneous or layered half-space. Such an approximate adjoint field is significantly faster to compute than the true adjoint field. This leads to a considerable reduction in computation time over the exact sensitivities. The speed-up can be one or two orders of magnitude, with the relative difference increasing with the size of the problem. Sensitivities calculated using the approximate adjoint field appear to be good approximations to the exact sensitivities. This is verified by comparing true and approximate sensitivities for 2- and 3-D conductivity models, and for sources that are both finite and infinite in extent. The approximation is sufficiently accurate to allow an iterative inversion algorithm to converge to the desired result, and we illustrate this by inverting magnetotelluric data to recover a 2-D conductivity structure. Our approximate sensitivities should enable larger inverse problems to be solved than is currently feasible using exact sensitivities and present-day computing power.

Key words: electromagnetic methods, Fréchet derivatives, inversion, magnetotellurics.

1 INTRODUCTION

Inverting electromagnetic measurements for a conductivity model of the Earth is a non-linear process. The classical approach is to linearize the problem and iterate towards the solution. Such linearized inversion schemes, whether as simple as the early approach of Jupp & Vozoff (1975) or as involved as, for example, that of deGroot-Hedlin & Constable (1990) or Oldenburg, McGillivray & Ellis (1993), all make use of the sensitivity, or Jacobian, matrix. The elements of this matrix, the 'sensitivities', are the partial derivatives of the data with respect to the model parameters,

$$J_{ij} = \frac{\partial d_i}{\partial m_j}, \qquad i = 1, \ldots, M, \qquad j = 1, \ldots, N, \tag{1}$$

where M is the number of measurements and N is the number of model parameters.

The three main methods of calculating the sensitivities are the brute-force or perturbation method, the sensitivity-equation method and the adjoint-equation method (McGillivray & Oldenburg 1990). The computation times for these methods are roughly equivalent to $N \times M_f$, $N \times M_f$ and $M_o \times M_f$ forward modellings, respectively, where M_f is the number of frequencies (or times), M_o is the number of observation locations ($M_f \times M_o = M$), and it is assumed that one forward modelling produces the electric field everywhere in the conductivity model for a single frequency (or time). Given $N > M$, which is the situation considered here, the adjoint-equation method is the most efficient.

It is sometimes possible to exploit features of a particular forward-modelling algorithm to reduce the time needed for one of the above methods. For example, Oristaglio & Worthington (1980) make use of the already-factored matrix from their finite-difference forward-modelling program when calculating the sensitivities using the sensitivity-equation method. Mackie & Madden (1993) use a conjugate gradient approach for solving the magnetotelluric inverse problem that does not explicitly need the Jacobian matrix but rather the product of this matrix with a given vector. This product can be efficiently calculated using their forward-modelling algorithm. Even so, as the size of the problem increases, the amount of com-

putations becomes such that exact sensitivities cannot be calculated within a reasonable time. In this paper we propose an approximate method for generating the Jacobian matrix that is considerably faster than any exact method, and yet is sufficiently accurate to allow an iterative inversion algorithm to converge to the solution.

Approximate sensitivities specifically designed for the inversion of magnetotelluric data have been used by Smith & Booker (1991) and by Ellis, Farquharson & Oldenburg (1993). These approximate sensitivities are based on the sensitivities for the 1-D magnetotelluric inverse problem. They are quick to compute and are a sufficiently good approximation to enable the successful inversion of magnetotelluric data for 2-D conductivity models. However, because these approximate sensitivities are based on the sensitivities for a 1-D model, they are not defined for cells that are not directly below the location of a particular measurement. The Jacobian matrix is therefore incomplete. The approximate sensitivities we present here give rise to a complete Jacobian matrix and are general enough to be used in the inversion of any electromagnetic measurements for any source–receiver configuration.

We first describe the adjoint-equation method of calculating precise sensitivities and then present our approximate form, covering in some depth the ways in which the adjoint electric field can be approximated. This forms the basis of our method. We then compare the exact and approximate sensitivities for 2- and 3-D conductivity models for various sources and measured quantities. We include an example inversion, using our approximate sensitivities, of a synthetic magnetotelluric data set for a 2-D model.

2 EXACT SENSITIVITIES

In our inverse problem the number of model parameters is considerably greater than the number of data, and the adjoint-equation method for calculating the sensitivities is the most efficient. This approach has been recognised by many investigators, e.g. Weidelt (1975), Park (1987), Madden & Mackie (1989), Madden (1990). Here we present the relevant equations as given by McGillivray *et al.* (1994).

Consider a domain, D, whose conductivity, σ, varies as a function of position, and whose electrical permittivity, ε, and magnetic susceptibility, μ, are constant. $\mathbf{J}_e$ and $\mathbf{J}_m$ are electric and magnetic sources. (The magnetic source is such that $\mathbf{J}_m = -i\omega\mu\mathbf{M}$, where $\mathbf{M}$ is the magnetization. This is consistent with Ward & Hohmann 1988 and Appendices B and C, for which unit electric and magnetic dipole sources correspond to $|\mathbf{J}_e| = 1$ and $|\mathbf{M}| = 1$, respectively.) The electric and magnetic fields, $\mathbf{E}$ and $\mathbf{H}$, respectively, that are generated in the domain by these sources are given by the frequency-domain Maxwell equations,

$$\nabla \times \mathbf{E} = -i\omega\mu\mathbf{H} + \mathbf{J}_m, \tag{2}$$

$$\nabla \times \mathbf{H} = (\sigma + i\omega\varepsilon)\mathbf{E} + \mathbf{J}_e, \tag{3}$$

and an appropriate set of boundary conditions. For the purposes of the inversion, the conductivity is represented as a finite linear combination of suitable basis functions,

$$\sigma(\mathbf{r}) = \sum_{j=1}^{N} \sigma_j \psi_j(\mathbf{r}), \tag{4}$$

where ψ_j are the basis functions and σ_j are coefficients. Substituting this representation into eqs (2) and (3), and differentiating with respect to σ_k, yields

$$\nabla \times \frac{\partial \mathbf{E}}{\partial \sigma_k} = -i\omega\mu \frac{\partial \mathbf{H}}{\partial \sigma_k}, \tag{5}$$

$$\nabla \times \frac{\partial \mathbf{H}}{\partial \sigma_k} = (\sigma + i\omega\varepsilon)\frac{\partial \mathbf{E}}{\partial \sigma_k} + \psi_k \mathbf{E}. \tag{6}$$

The partial derivatives $\partial\mathbf{E}/\partial\sigma_k$ and $\partial\mathbf{H}/\partial\sigma_k$ are the sensitivities of the electric and magnetic fields with respect to the coefficient σ_k. These sensitivities satisfy the homogeneous form of the possibly inhomogeneous boundary conditions that $\mathbf{E}$ and $\mathbf{H}$ satisfy.

To arrive at a numerical method for calculating the sensitivities, a suitable solution to eqs (5) and (6) has to be found. Consider an auxiliary problem in which auxiliary electric and magnetic fields, $\mathbf{E}^\dagger$ and $\mathbf{H}^\dagger$, are generated in the domain D by as yet undefined electric and magnetic sources $\mathbf{J}_e^\dagger$ and $\mathbf{J}_m^\dagger$. These auxiliary fields satisfy the following version of Maxwell's equations:

$$\nabla \times \mathbf{E}^\dagger = -i\omega\mu\mathbf{H}^\dagger + \mathbf{J}_m^\dagger, \tag{7}$$

$$\nabla \times \mathbf{H}^\dagger = (\sigma + i\omega\varepsilon)\mathbf{E}^\dagger + \mathbf{J}_e^\dagger. \tag{8}$$

The auxiliary fields are required to satisfy homogeneous boundary conditions that need not be the same as those satisfied by the sensitivities if the domain boundary, ∂D, extends to infinity, but must be the same as those satisfied by the sensitivities if the domain is finite (see McGillivray *et al.* 1994). Given this auxiliary problem, it can be shown that

$$\int_D \left(\mathbf{J}_m^\dagger \cdot \frac{\partial \mathbf{H}}{\partial \sigma_k} + \mathbf{J}_e^\dagger \cdot \frac{\partial \mathbf{E}}{\partial \sigma_k} \right) dv = \int_D \mathbf{E}^\dagger \cdot \mathbf{E}\, \psi_k \, dv. \tag{9}$$

This is the fundamental equation: the sensitivities for the electric and magnetic fields can be determined from this equation by an appropriate choice of sources, $\mathbf{J}_e^\dagger$ and $\mathbf{J}_m^\dagger$, for the auxiliary problem. For example, to obtain the sensitivity at an observation location $\mathbf{r}_o$ for the x-component of the electric field, choose $\mathbf{J}_e^\dagger = \delta(\mathbf{r} - \mathbf{r}_o)\hat{\mathbf{e}}_x$ and $\mathbf{J}_m^\dagger = 0$. Substituting these expressions into eq. (9) gives

$$\left. \frac{\partial E_x}{\partial \sigma_k} \right|_{\mathbf{r}_o} = \int_D \mathbf{E}^\dagger \cdot \mathbf{E}\, \psi_k \, dv. \tag{10}$$

For this example, the auxiliary electric field, $\mathbf{E}^\dagger$, is now defined as the electric field in the domain due to an x-directed unit electric dipole at the location $\mathbf{r}_o$ at which the observation of E_x was made. $\mathbf{E}$ is the electric field generated in the domain due to the particular source (described by $\mathbf{J}_e$ and $\mathbf{J}_m$) used in the geophysical survey.

Eq. (9) can be obtained by a formal Green's function solution of eqs (5) and (6) for the sensitivities. It is found that the auxiliary electric field, $\mathbf{E}^\dagger$, above is equivalent to the complex conjugate of the appropriate adjoint Green's function for eqs (5) and (6). We shall therefore use the term 'adjoint field', rather than 'auxiliary electric field', to refer to $\mathbf{E}^\dagger$.

3 APPROXIMATE SENSITIVITIES

In order to calculate the sensitivities using eq. (9) we need to: (1) compute the electric field, $\mathbf{E}$, due to the source used in the geophysical experiment; (2) compute the adjoint field, $\mathbf{E}^\dagger$, due to the appropriate dipole source at the observation location; and (3) evaluate the volume integral of the inner product of these two fields. The computation time for the numerical

integration is negligible compared to any forward modelling. Also, in an iterative inversion algorithm, the electric field, **E**, will already have been computed in order to calculate the data misfit for the previous iteration. The majority of the computation time for this method of calculating the sensitivities is therefore due to the calculation of the adjoint field for a dipole source at each observation location.

For our approximate sensitivities we generate an approximation to $\mathbf{E}^\dagger$ instead of computing this adjoint field in the true multidimensional conductivity model. As examples we use the electric field in a homogeneous half-space due to the appropriate dipole source or that in a horizontally layered half-space. Not only are such approximate adjoint fields much quicker to compute than the true adjoint field, but they need only be explicitly generated for one dipole location and then translated horizontally for all other dipole locations. This leads to considerable time savings in the generation of the Jacobian matrix. The Born approximation of the adjoint field is also considered, but its increased computation time over the two approximations discussed above makes its usefulness debatable.

The approximate sensitivities we present here are similar to those in the Born iterative method (e.g. Sena & Toksöz 1990; Alumbaugh & Morrison 1995). However, unlike the Born iterative method in which the Green's function, or the adjoint field $\mathbf{E}^\dagger$ in the notation of eq. (9), remains unchanged throughout the iterative inversion process and only the electric field, **E**, is updated, our approximate adjoint field is modified at each iteration in response to the current conductivity model. The homogeneous or layered half-space in which the approximate adjoint field is computed is obtained from a weighted average of the conductivities (or the logarithms of the conductivities) of all the cells in the current conductivity model, or from the weighted averages of the cells in each horizontal row or plane of the current model.

The approximate adjoint fields mentioned above will obviously not contain all the features of the true adjoint field in the multidimensional model. However, as we shall illustrate in the next section, the true adjoint field is dominated by its decay away from the dipole source. Suitable choices of conductivities for the homogeneous or layered half-space result in an approximate adjoint field that has the same dominant behaviour, and approximate sensitivities that seem to be sufficiently accurate to allow an iterative inversion procedure to converge.

To provide substance to the above statements we compare our approximate sensitivities with the true sensitivities for 2-, 2.5- and 3-D situations. The close comparisons that are obtained do not prove that the approximate sensitivities will work for all inversions of electromagnetic data, but they do provide optimism about their utility.

4 EXAMPLES

In the following sections we investigate the merits of our sensitivities for 2-, 2.5- and 3-D problems. The study is not exhaustive since results are model-dependent. Rather, the intention is to illustrate the applicability of the approximate sensitivities. We first compare possible forms of the approximate adjoint field with the true adjoint field for a purely 2-D problem, and then compare the corresponding approximate sensitivities with the true sensitivities for the 2-D magnetotelluric inverse problem. We use these approximate sensitivities in an inversion of synthetic magnetotelluric data for a simple 2-D model. Finally, we consider the approximate sensitivities for controlled-source configurations over a 2-D model and a 3-D model. Mathematical derivations of the various adjoint fields are mostly relegated to appendices.

4.1 Approximate adjoint fields for a simple 2-D example

Consider the 2-D conductivity model shown in Fig. 1(a) comprising a conductive block of $0.1\ \mathrm{S\,m^{-1}}$ buried in a more resistive background of $0.01\ \mathrm{S\,m^{-1}}$, and overlying a conductive basement of $0.1\ \mathrm{S\,m^{-1}}$. Suppose measurements are made of the electric and magnetic fields induced in this model by a source that is also invariant in the strike direction (for example, the plane-wave source assumed in magnetotelluric surveys). For this purely 2-D problem, the adjoint field is the electric field due to a 2-D dipole source at the measurement location (see Appendix A). This source is equivalent to an infinite line of point dipoles that is parallel to the strike direction and that passes through the measurement location. Suppose a measurement of the along-strike electric field, E_y, has been made at $x_o = -3000$ m on the surface of the model. The sensitivity of this measurement with respect to the model parameter σ_k is given by

$$\left.\frac{\partial E_y}{\partial \sigma_k}\right|_{x_o=-3000} = \int_A \mathbf{E}^\dagger \cdot \mathbf{E}\,\psi_k\,ds. \tag{11}$$

Here, the adjoint field, $\mathbf{E}^\dagger$, is the electric field due to a unit 2-D y-directed electric dipole source at the observation location $x_o = -3000$ m. The true adjoint field for this model was computed using the finite-element code of Unsworth, Travis & Chave (1993). The amplitude of this adjoint field is shown in Fig. 2(a), and the phase in Fig. 3(a). The frequency of the source was 0.2 Hz. Note the slight distortion of the phase due to the conductive block, and the increased decay of the amplitude and the increase in the phase as the electric field penetrates the conductive basement.

We now present three forms of the approximate adjoint field: that computed in a homogeneous half-space; that in a layered half-space; and that using the Born approximation. In each case the source is the 2-D y-directed electric dipole at $x_o = -3000$ m.

4.1.1 *Homogeneous half-space*

The method used for computing the electric field generated in the homogeneous half-space by a 2-D dipole source is briefly described in Appendix B. Fig. 2(b) shows the amplitude and Fig. 3(b) shows the phase of the electric field computed in a homogeneous half-space of $0.028\ \mathrm{S\,m^{-1}}$ (the average of the logarithm of the conductivity, weighted by cross-sectional area, for the model in Fig. 1a) for a 2-D, y-directed electric dipole source at $x_o = -3000$ m, and for a frequency of 0.2 Hz. This is the approximate adjoint field that would be used in place of the true adjoint field shown in Figs 2(a) and 3(a).

The approximate adjoint field shown in Figs 2(b) and 3(b) obviously contains no information about the conductive block nor the conductive basement. However, the dominant behaviour of the true adjoint field shown in Figs 2(a) and 3(a) is the decay in amplitude and increase in phase away from the source, which is exactly the behaviour of the approximate adjoint field in Figs 2(b) and 3(b). The effect of the 2-D

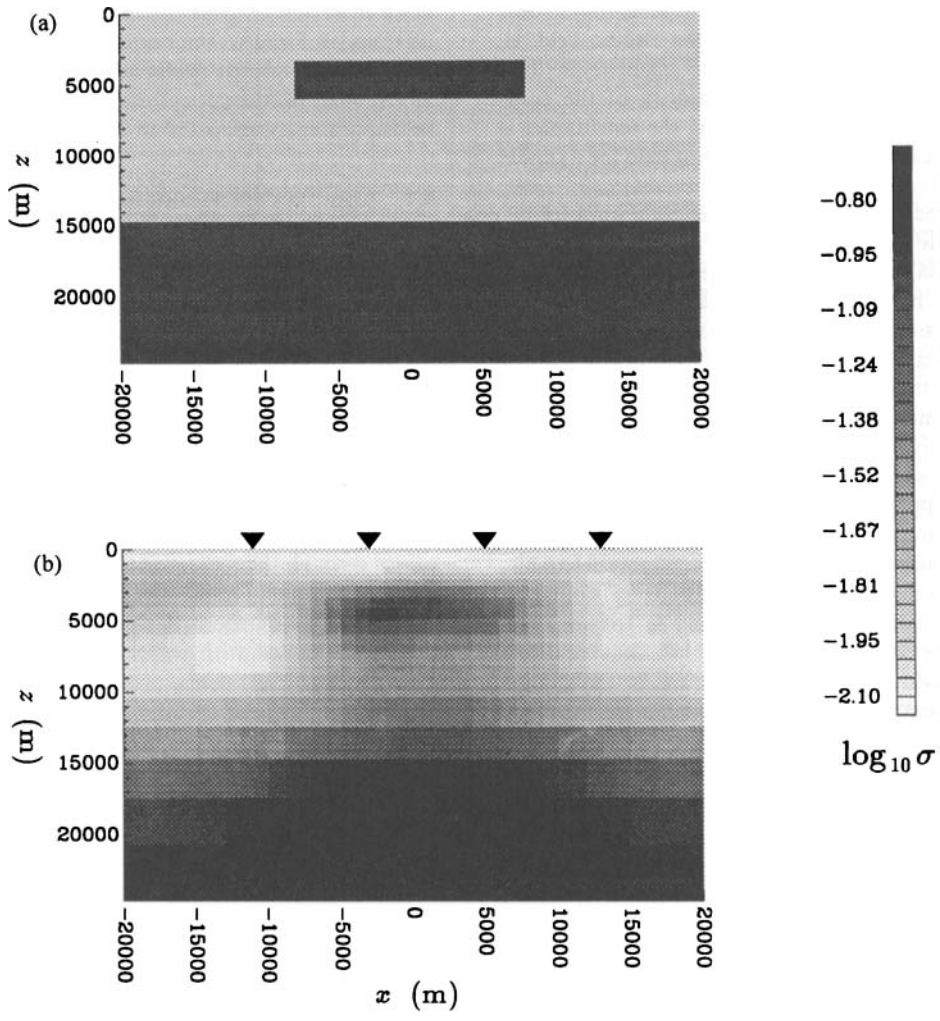

Figure 1. (a) The 2-D conductivity model used throughout this paper to illustrate the approximate adjoint fields and approximate adjoint sensitivities. (b) The final model produced by the inversion of synthetic MT data in Section 4.2. The triangles indicate the observation locations.

structure in the conductivity model shown in Fig. 1(a) can almost be relegated to a perturbation of the field that would otherwise be present in the homogeneous half-space. It is this level of agreement between true and approximate adjoint fields that we feel is important for the subsequent approximate sensitivities to be useful in an iterative inversion scheme.

4.1.2 *Layered half-space*

The second form of the approximate adjoint field is that computed in a layered half-space. An appropriate layered half-space could be constructed by averaging the conductivity of the multidimensional model in each of a series of horizontal layers. The electric field generated in such a layered model by a 2-D source can be computed using the method described in Appendix C. Doing this for a y-directed electric dipole at $x_0 = -3000$ m and for a frequency of 0.2 Hz gives the electric field shown in Figs 2(c) and 3(c). The layered half-space used for this example was obtained by averaging the logarithm of the conductivity, weighted by the across-strike area, in each horizontal layer of the model in Fig. 1(a). Just as for the approximate adjoint field computed in a homogeneous half-space [see Figs 2(b) and 3(b)], there is no manifestation in the field shown in Figs 2(c) and 3(c) of the 2-D effects of the conductive block. However, the rapid decrease in amplitude and increase in phase of the true adjoint field in the conductive basement [see Figs 2(a) and 3(a)] are well reproduced in the approximate adjoint field computed in the layered half-space. This is not surprising since this feature of the 2-D model is replicated in the layered half-space used for computing the approximate adjoint field.

4.1.3 *Born approximation*

The third form of the approximate adjoint field that we present is based on a Born approximation. Consider the integral equation describing the true adjoint field, $\mathbf{E}^\dagger$, in the multidimensional conductivity model [eq. (27), Hohmann (1988)]:

$$\mathbf{E}^\dagger(\mathbf{r}) = \mathbf{E}^\dagger_p(\mathbf{r}) + \int_D \mathbf{G}(\mathbf{r};\mathbf{r}')\cdot\mathbf{E}^\dagger(\mathbf{r}')\Delta\sigma(\mathbf{r}')\,dv', \tag{12}$$

where $\mathbf{E}^\dagger_p$ is the electric field calculated in some background conductivity model and $\Delta\sigma$ is the difference between the background and true conductivity structures. $\mathbf{G}$ is the tensor Green's function for the background conductivity model.

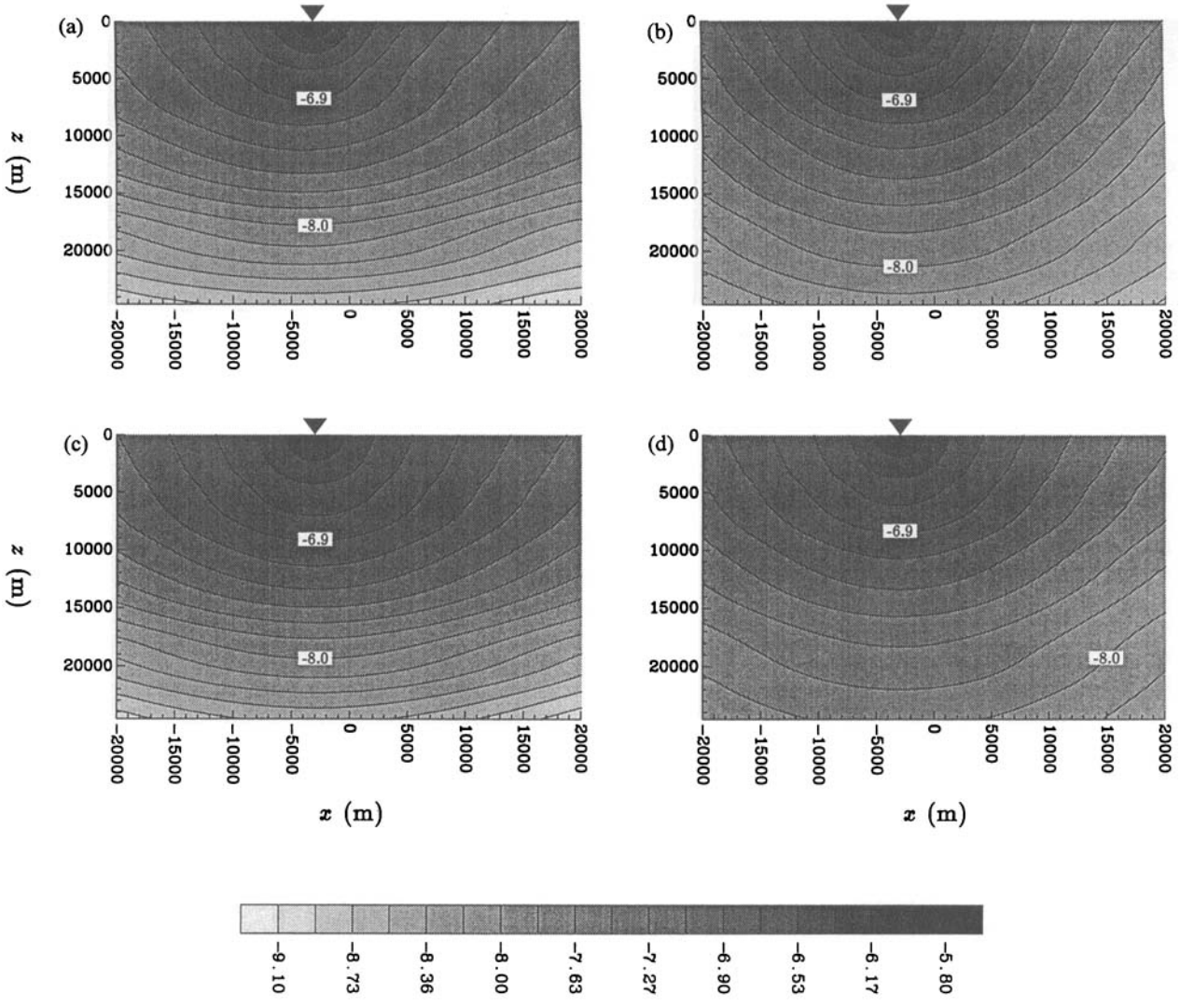

Figure 2. The amplitudes of the true and approximate adjoint fields for a y-directed electric line source over the 2-D conductivity model shown in Fig. 1(a). The location of the line source is shown by the triangle. Panel (a) shows the true adjoint field, and panels (b) to (d) show, respectively, the approximate adjoint fields computed in a homogeneous half-space, in a layered half-space, and using the Born approximation. The grey-scale represents $\log_{10}|E|$.

Eq. (12) above is exact. The Born approximation for $\mathbf{E}^\dagger$ is obtained by replacing $\mathbf{E}^\dagger$ in the integrand by $\mathbf{E}_p^\dagger$,

$$\mathbf{E}^\dagger(\mathbf{r}) \approx \mathbf{E}_p^\dagger(\mathbf{r}) + \int_D \boldsymbol{G}(\mathbf{r};\mathbf{r}') \cdot \mathbf{E}_p^\dagger(\mathbf{r}') \Delta\sigma(\mathbf{r}')\, dv'. \tag{13}$$

The elements of the tensor Green's function,

$$\boldsymbol{G}(\mathbf{r};\mathbf{r}') = \begin{pmatrix} G_{xx} & G_{xy} & G_{xz} \\ G_{yx} & G_{yy} & G_{yz} \\ G_{zx} & G_{zy} & G_{zz} \end{pmatrix}, \tag{14}$$

are such that G_{xy} is the x-component of the electric field generated in the background conductivity model by a unit y-directed electric dipole. For a 2-D source and a 2-D conductivity model, the electromagnetic induction problem breaks down into two decoupled modes: one in which there is only an along-strike component of the electric field ('E-polarization' or 'TE' mode), and one in which the electric field is completely in the plane perpendicular to the strike direction ('H-polarization' or 'TM' mode). For the E-polarization case, eq. (13) reduces to a scalar equation and the only relevant component of the tensor Green's function, G_{yy}, for a homogeneous background is given by Hohmann (1988). For the H-polarization case, the relevant components of the tensor Green's function for a homogeneous background are given by Lee & Morrison (1984).

The Born approximation for the adjoint field was calculated for the conductivity model in Fig. 1(a). The background conductivity model in which $\mathbf{E}_p^\dagger$ and $\boldsymbol{G}$ were calculated was a homogeneous half-space of 0.01 S m^{-1}. This value was chosen over that used for the homogeneous half-space described in section 4.1.1 so that the integration in eq. (13) was evaluated over the smallest possible number of cells. The resulting approximate adjoint field generated by a 2-D y-directed electric dipole source is shown in Figs 2(d) and 3(d). As before, a frequency of 0.2 Hz was used. From Figs 2(d) and 3(d) it can be seen that the Born approximation produces a poorer approximation of the amplitude of the adjoint field than that

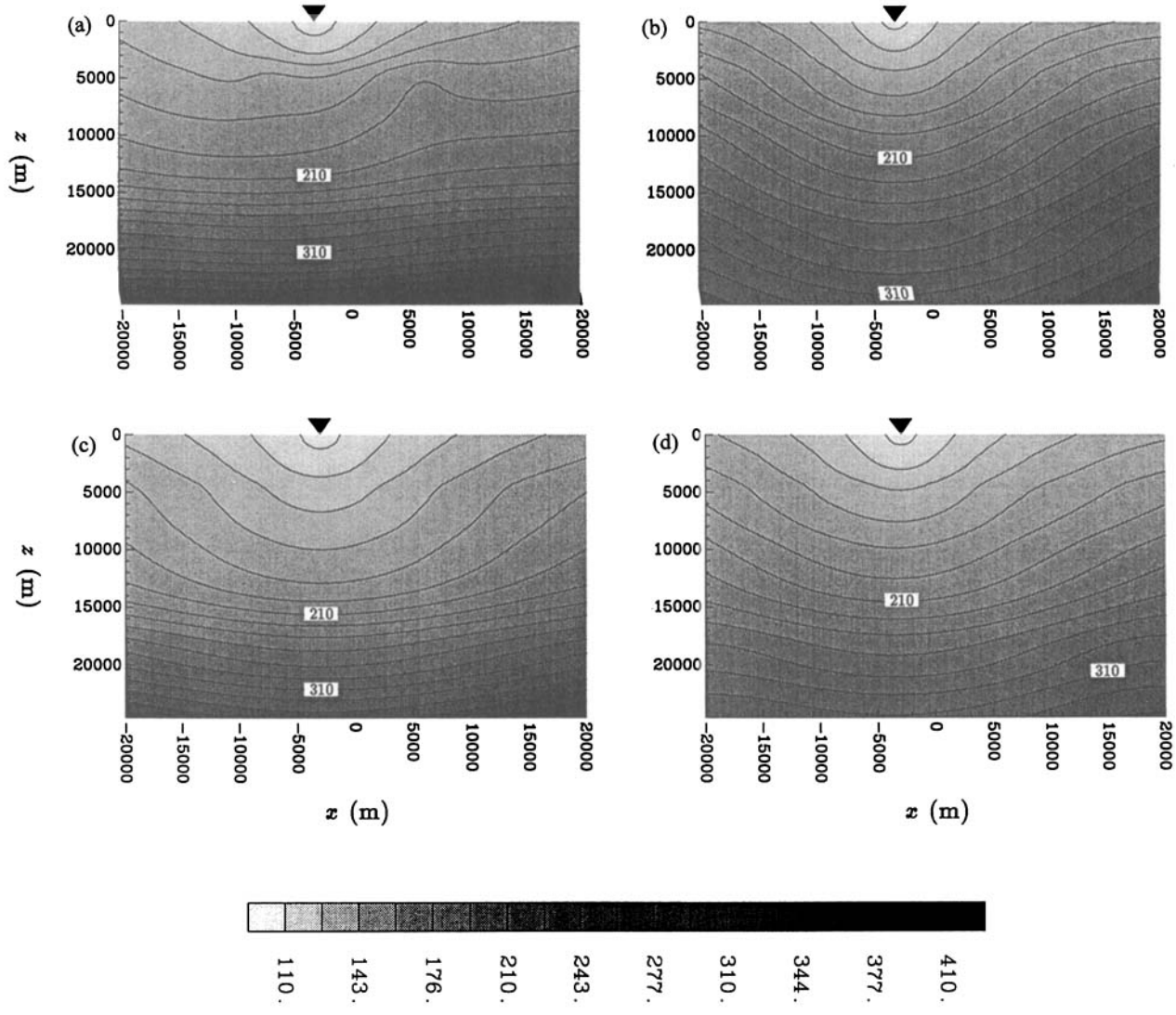

Figure 3. The phases of the true and approximate adjoint fields for the 2-D conductivity model shown in Fig. 1(a). The location of the line source is shown by the triangle. Panel (a) shows the true adjoint field, and panels (b) to (d) show, respectively, the approximate adjoint fields computed in a homogeneous half-space, in a layered half-space, and using the Born approximation. The grey-scale represents phase in degrees.

computed in the homogeneous half-space. This is because of the difference between the background conductivity used to compute the Born approximation and the conductivity of the homogeneous half-space used to produce Figs 2(b) and 3(b). However, the phase of the Born approximation (Fig. 3d) is somewhat better than that computed for the homogeneous half-space above about 1000 m depth and does give an indication of the increase in phase that the true adjoint field exhibits in the conductive basement, although this is not reproduced nearly as well as in the approximation calculated in the layered model.

4.1.4 Computation times

The true and approximate adjoint fields described above were computed on a Sun Sparc10 workstation. The time required to compute each of these is listed in Table 1. For the given values, the adjoint field was computed at 861 nodes (21 vertically and 41 horizontally) for the 2-D y-directed electric dipole source. The approximate adjoint fields calculated in a homogeneous or layered half-space have similar computation times that are significantly less than the computation time for the true adjoint field. The Born approximation takes considerably longer to compute than the true adjoint field. This is because the Green's function needed in eq. (13), that is the electric field in the homogeneous half-space due to a 2-D electric dipole, has to be computed for dipoles at depths within the model, not just for one source at the surface.

Table 1. Example computation times for the various types of 2–D adjoint fields.

True adjoint field		7 s
Approximate adjoint field:	homogeneous half-space	1 s
	layered half-space	2 s
	Born approximation	25 s

4.2 Approximate sensitivities for the 2-D magnetotelluric inverse problem

We have thus far compared three approximate forms of the adjoint field that could be used for a purely 2-D inverse

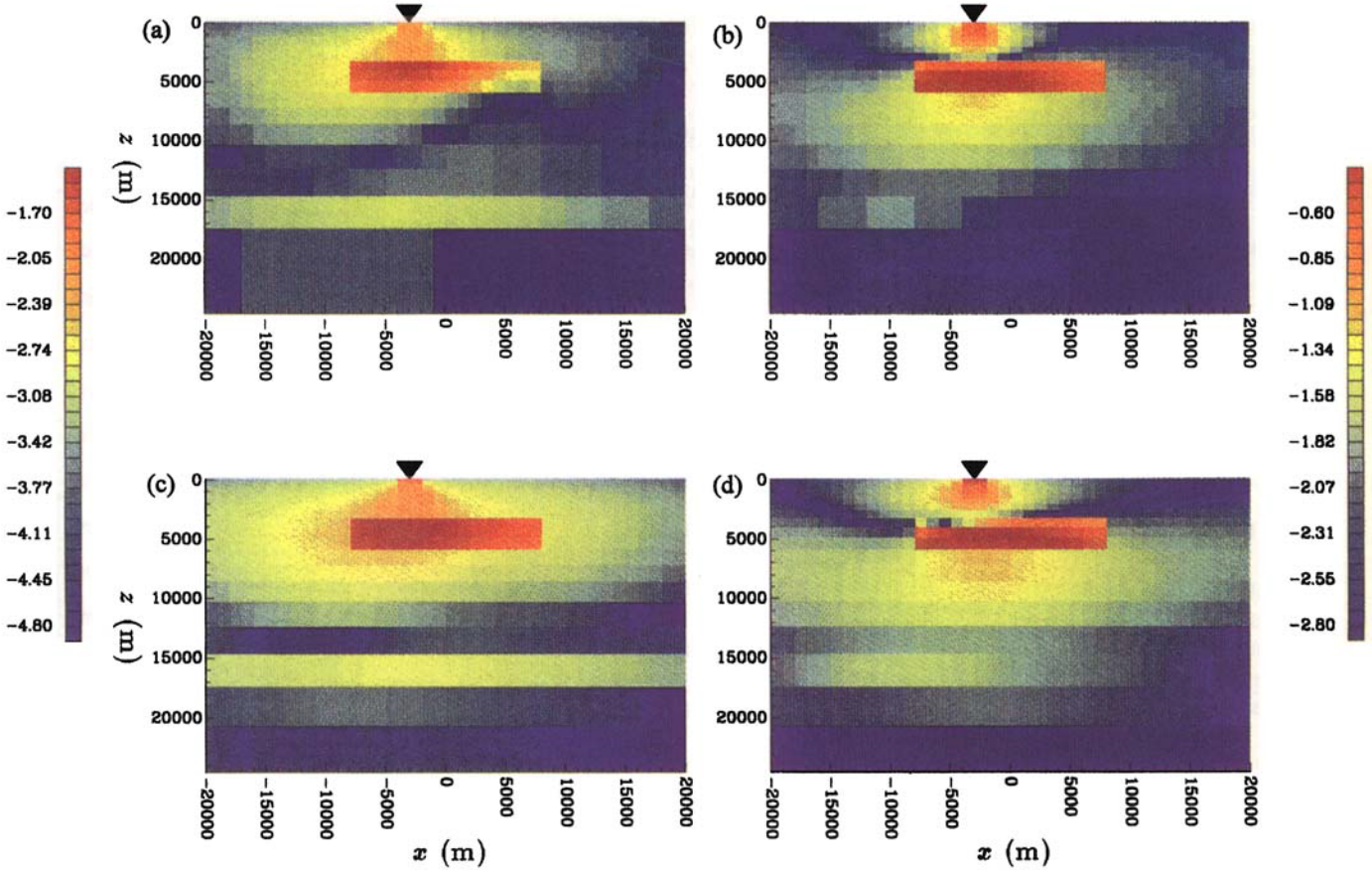

Figure 4. Brute-force and approximate sensitivities for the E-polarization apparent resistivity and phase for the conductivity model shown in Fig. 1(a). The observation location is indicated by the triangle. Panels (a) and (c), and the colour bar on the left of the figure, show $\log_{10}|\partial \ln \rho_a / \partial \ln \sigma|$, and panels (b) and (d), and the colour bar on the right show $\log_{10}|\partial \phi / \partial \ln \sigma|$. Panels (a) and (b) show the sensitivities produced by the brute-force method, and panels (c) and (d) show the approximate sensitivities calculated using the approximate adjoint field computed in a layered half-space.

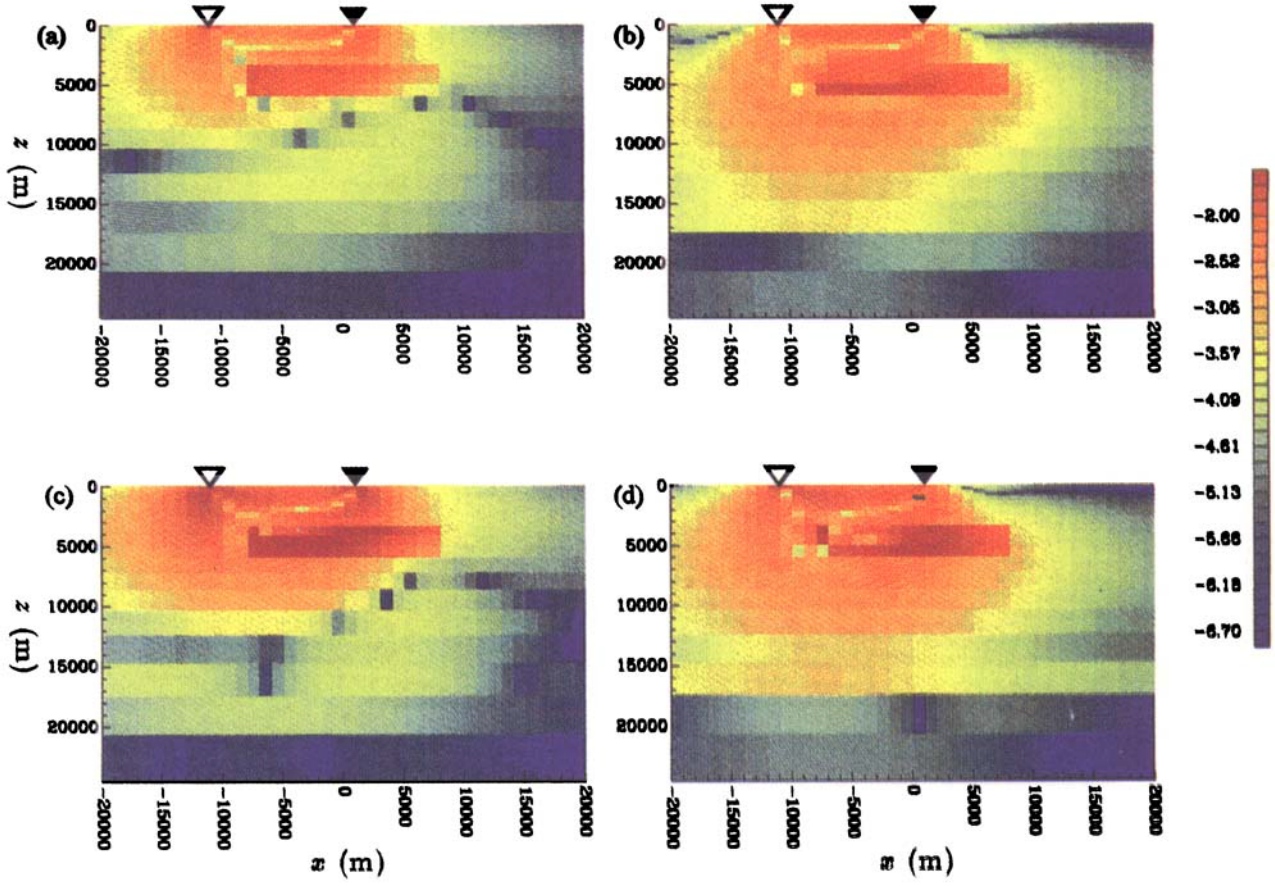

Figure 6. 2.5-D sensitivities for the conductivity model shown in Fig. 1(a) and for the experimental configuration considered in Section 4.3. The source and observation locations are indicated by the open and solid triangles, respectively. Panels (a) and (c) show $\log_{10}|\partial \ln |E|/\partial \ln \sigma|$, and panels (b) and (d) show $\log_{10}|\partial\phi/\partial \ln \sigma|$. The colour bar refers to all four panels. Panels (a) and (b) were produced by the adjoint-equation method, and panels (c) and (d) were produced by the approximate-sensitivity program using an adjoint field computed in a layered half-space.

problem. In this section we use these approximate adjoint fields to calculate the approximate sensitivities for the 2-D magnetotelluric problem.

4.2.1 *The approximate sensitivities*

The observed quantities in a magnetotelluric experiment are usually the frequency-domain values of apparent resistivity, ρ_a, and phase, ϕ. For a 2-D earth, for which the magnetotelluric problem can be split into two decoupled modes, the apparent resistivity and phase for the E-polarization mode are given by

$$\rho_a(\omega) = \frac{1}{\omega\mu}\left|\frac{E_y}{H_x}\right|^2 \quad \text{and} \quad \phi(\omega) = \text{phase}\left(\frac{E_y}{H_x}\right), \tag{15}$$

and for the H-polarization mode by

$$\rho_a(\omega) = \frac{1}{\omega\mu}\left|\frac{E_x}{H_y}\right|^2 \quad \text{and} \quad \phi(\omega) = \text{phase}\left(\frac{E_x}{H_y}\right), \tag{16}$$

where ω is the angular frequency and μ is the magnetic permeability. The strike direction is assumed to be the y-direction. The sensitivities for the apparent resistivity and phase can be expressed in terms of the sensitivities for the electric and magnetic fields (see Appendix D),

$$\frac{\partial \rho_a}{\partial \sigma_j} = 2\rho_a\left[\mathcal{R}e\left(\frac{1}{E}\frac{\partial E}{\partial \sigma_j}\right) - \mathcal{R}e\left(\frac{1}{H}\frac{\partial H}{\partial \sigma_j}\right)\right] \tag{17}$$

and

$$\frac{\partial \phi}{\partial \sigma_j} = \mathcal{I}m\left(\frac{1}{E}\frac{\partial E}{\partial \sigma_j}\right) - \mathcal{I}m\left(\frac{1}{H}\frac{\partial H}{\partial \sigma_j}\right). \tag{18}$$

Approximate sensitivities for the apparent resistivity and phase can therefore be generated from the adjoint-equation method discussed in Section 2 using one of the approximate forms of the adjoint field described in Section 4.1.

We illustrate this by calculating the approximate sensitivities for the conductivity model shown in Fig. 1(a). Suppose measurements of apparent resistivity and phase had been made at $x_o = -3000$ m on the surface of the model at a frequency of 0.2 Hz. The conductivity model was divided into 800 cells (20 vertically and 40 horizontally), the conductivity constant in each of these cells. The 'exact' sensitivities were calculated using the brute-force (or perturbation) method: the conductivity of each cell was perturbed in turn by 1 per cent and a forward modelling performed, using a transmission surface modelling code (Madden 1972), to calculate the resulting change in the apparent resistivity and phase. The sensitivity with respect to the perturbed model parameter is then given by the change in the apparent resistivity or phase divided by the change in the model parameter. These brute-force sensitivities for the E-polarization apparent resistivity and phase are shown in Figs 4(a) and (b). Fig. 4(a) shows the sensitivity of the apparent resistivity at $x_o = -3000$ m for a frequency of 0.2 Hz with respect to the conductivities of the 800 cells in the model. The sensitivity is plotted as a constant value over the area of the cell to which the sensitivity corresponds. Fig. 4(b) shows the sensitivity of the phase in a similar manner.

Approximate sensitivities were calculated using the approximate adjoint field computed in a layered half-space. The resulting approximate sensitivities for the E-polarization apparent resistivity and phase (for $x_o = -3000$ m and a frequency of 0.2 Hz) are shown in Figs 4(c) and (d). Comparison of the panels of Fig. 4 indicates a good agreement between the approximate and exact sensitivities.

4.2.2 *Computation times*

Table 2 lists the computation times for the various methods of calculating the matrix of sensitivities for a small 2-D magnetotelluric example. The sensitivities were calculated for 80 data (observations of apparent resistivity and phase for both E- and H-polarizations at four locations and at five frequencies) with respect to the conductivities of the 800 cells used to parametrize the model in Fig. 1(a). The approximate adjoint fields in both the homogeneous and layered half-spaces were only explicitly computed for one observation location and then translated horizontally to calculate the sensitivities for the three remaining observation locations. This results in a considerable time saving that becomes more significant with increasing numbers of observation locations. In a similar manner, for the Born approximation of the adjoint field, both $\mathbf{E}_p^\dagger$ and $\boldsymbol{G}$, which were calculated in a homogeneous half-space, were explicitly computed for only the first observation location and then translated horizontally for the other three observation locations. This reduces the computation time for this third form of approximate sensitivities, although it is still not less than that of the exact sensitivities. It is not until there are tens of observation locations that this form of approximate sensitivities requires less time to calculate than the exact sensitivities.

Table 2. Example computation times for the various types of sensitivities for the 2-D magnetotelluric inverse problem.

Exact sensitivities:	brute-force	500 min
	adjoint equation	2.5 min
Approximate sensitivities:	homogeneous half-space	0.25 min
	layered half-space	0.5 min
	Born approximation	5 min

4.2.3 *Inversion of synthetic data*

The approximate sensitivities described above, calculated using the approximate adjoint field in a layered half-space, were used to invert a set of synthetic data generated from the conductivity model in Fig. 1(a). Values of the E- and H-polarization apparent resistivities and phases were calculated at four observation locations ($x_o = -11\,000$, -3000, 5000 and 13 000 m) for five frequencies (1, 0.5, 0.2, 0.1 and 0.05 Hz). Gaussian random noise of zero mean was added to these data. The standard deviation of the noise added to the apparent resistivity was 5 per cent, and that added to the phase was 2°. These 80 data were inverted using an iterative, linearized inversion procedure in which the system of equations at each iteration was solved using a subspace technique. For the inversion, the data were considered to be the phase and the logarithm of the apparent resistivity. The details of the inversion algorithm are given in Oldenburg & Ellis (1993). The model norm that was minimized was the discrete equivalent of

$$\phi_m = \int_D \left[\alpha_s w_s (m - m_0)^2 + \alpha_x w_x \left(\frac{\partial (m - m_0)}{\partial x}\right)^2 + \alpha_z w_z \left(\frac{\partial (m - m_0)}{\partial z}\right)^2\right] dv, \tag{19}$$

where the model, m, was equal to $\ln \sigma$, and the reference model,

m_0, corresponded to a half-space of conductivity 0.01 S m^{-1}. The values of the coefficients were $\alpha_s = 10^{-3}$, $\alpha_x = 3$ and $\alpha_z = 1$. The weighting functions, w_s, w_x and w_z were constant and equal to unity throughout the model domain. The subspace vectors were the steepest descent vectors,

$$\mathbf{v}_k = (\mathbf{W}_m^T \mathbf{W}_m)^{-1} \nabla_m \phi_d^k, \qquad k = 1, \ldots, 20, \tag{20}$$

where $\mathbf{W}_m$ is the weighting matrix associated with the discrete equivalent of eq. (19), and ϕ_d^k is the data misfit for the kth partition of the data. The data were ordered according to their individual misfit and then divided into 20 partitions.

The final model is shown in Fig. 1(b). The conductive block has approximately the correct amplitude and is situated at the correct depth and horizontal location. The conductive basement has also been recovered. Differences between this model and the true model in Fig. 1(a) are attributable to finding a smooth conductivity structure that reproduces the rather small data set worked with here. The values of the data misfit, ϕ_d, and model norm, ϕ_m, during the inversion are shown in Fig. 5. The algorithm was asked to decrease the misfit by a factor of 0.8 at each iteration, and this it managed for the first 17 iterations. The algorithm could then only decrease the misfit more slowly than the requested rate. The target misfit of 80 is achieved after 31 iterations. The model norm gradually increases before levelling off once the algorithm has achieved the target data misfit.

4.3 Approximate sensitivities for the 2.5-D electromagnetic inverse problem

The previous two sections dealt with the purely 2-D inverse problem. We shall now consider the 2.5-D problem in which the conductivity model is 2-D and the source field varies in three dimensions.

Consider the 2-D conductivity model shown in Fig. 1(a), and consider a controlled-source electromagnetic experiment in which an along-strike electric dipole source is located at $x_s = -11\,000$ m and $y_s = z_s = 0$. Suppose measurements are made of the along-strike component of the electric field at $x_o = 1100$ m and $y_o = z_o = 0$, and at a frequency of 0.2 Hz. The exact sensitivities for this arrangement were calculated by both

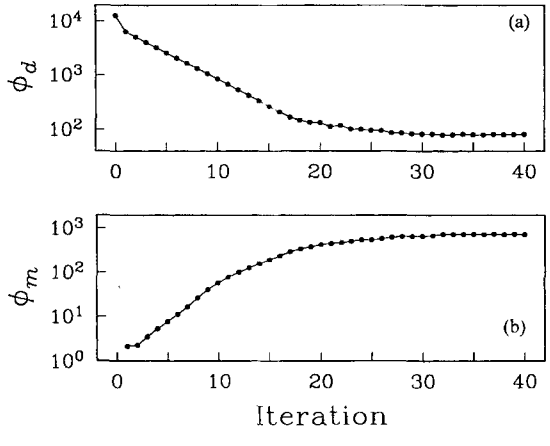

Figure 5. The data misfit, ϕ_d, and model norm, ϕ_m, as functions of iteration during the inversion of the synthetic magnetotelluric data set using the approximate sensitivities. The resulting model is shown in Fig. 1(b).

the brute-force method using the forward-modelling program of Unsworth *et al.* (1993) and the adjoint-equation method (Unsworth & Oldenburg 1995). Fig. 6(a) shows the exact sensitivities (calculated using the latter method) of the natural logarithm of the amplitude of the electric field with respect to the logarithms of the conductivities of each of the 800 cells in the model. Fig. 6(b) shows the sensitivities for the phase with respect to the logarithms of the conductivities of the cells.

Approximate sensitivities were calculated using an approximate adjoint field computed in a layered half-space. This adjoint field was computed using the method described in Appendix C. As in Section 4.1, the layered half-space was obtained by averaging the logarithm of the conductivities of the cells, weighted by their across-strike area, in each horizontal layer of the model in Fig. 1(a). The numerical integration over each cell was carried out in the along-strike-wavenumber domain (Unsworth & Oldenburg 1995). The resulting approximate sensitivities are shown in Figs 6(c) and (d) and are in good agreement with the exact sensitivities.

The computation times for the exact and approximate sensitivities described above for the small 2.5-D example are listed in Table 3. These times are for observations of the amplitude and phase of the along-strike electric field at six observation locations at a frequency of 0.2 Hz and for the 800 cells in the model.

Table 3. Example computation times for the exact and approximate sensitivities for the 2.5-D inverse problem.

Exact sensitivities: brute-force	5000 min
adjoint equation	25 min
Approximate sensitivities: layered half-space	5 min

4.4 Approximate sensitivities for a 3-D experiment

In this final section we consider the approximate sensitivities for the 3-D controlled-source problem. The comparison of approximate and exact sensitivities was severely restricted, however, by the limitations placed on 3-D forward modelling.

Consider the experimental configuration shown in Fig. 7, consisting of a grounded wire source extending from (50, −5, 0) m to (50, 5, 0) m, and measurements of the vertical component of the H-field at (0, 750, 0) m. The frequency was 100 Hz. The region extending from $x = 400$ to 650 m, from $y = -100$ to 150 m and from $z = 0$ to 250 m was discretized into $5 \times 5 \times 5$ cuboidal cells as shown in Fig. 7. The conductivity model comprised a conductive block of 0.1 S m^{-1} in a background of 0.01 S m^{-1}. The conductive block coincides with the shaded cells in Fig. 7. Brute-force sensitivities were calculated using the forward-modelling program SAMAYA (Gupta, Raiche & Sugeng 1989). The resulting sensitivities for the third vertical plane (perpendicular to the x-direction) of cells from the source are shown in Figs 8(a) and (b).

Approximate sensitivities were calculated for the model and experimental configuration described above using the approximate adjoint field in a layered half-space. These sensitivities are shown in Figs 8(c) and (d). There is, in general, good agreement between the brute-force and approximate sensitivities shown in Fig. 8, although there are differences between the sensitivities of the phase for the cells outside the conductive block, especially in the second row. However, the resolution of the comparison is poor because of the limited number of cells in the model.

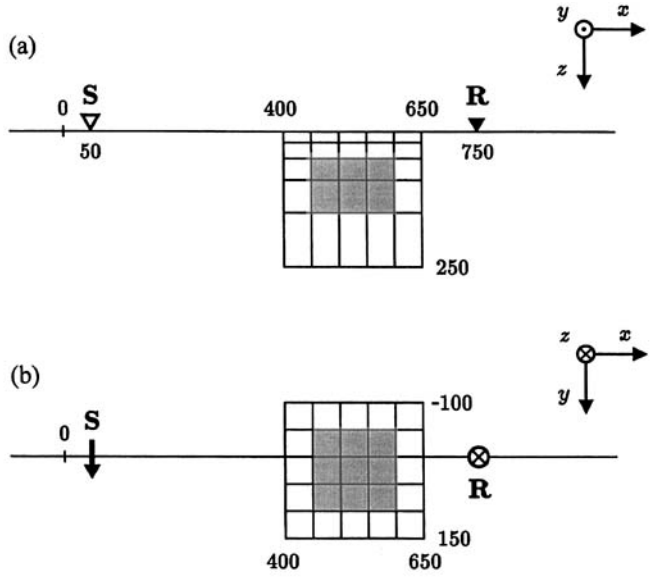

Figure 7. Geometry for the 3-D example considered in Section 4.4. Panel (a) is the side view and panel (b) is the plane view. **S** indicates the y-directed grounded wire source and **R** indicates the observation location. The shaded cells show the location of the conductive block. The numbers correspond to distances in metres.

The computation times for the brute-force and approximate sensitivities for the small 3-D example described above are shown in Table 4. Six observation locations were considered at the single frequency of 100 Hz. An estimated time for the adjoint-equation method is also given. This estimate is equal to the time required to carry out six forward modellings for this test-case using SAMAYA. Even for this small example the approximate sensitivities are almost two orders of magnitude faster to compute than the exact sensitivities. This time-difference will increase further as the number of observation locations increases.

Table 4. Example computation times for the exact and approximate sensitivities for the 3-D inverse problem.

Exact sensitivities: brute-force	260 min
adjoint-equation	12 min
Approximate sensitivities: layered half-space	10 s

5 CONCLUSIONS

In this paper we have presented a form of approximate sensitivities that is appropriate for use in a linearized, iterative method for inverting electromagnetic data. These approximate sensitivities are obtained by replacing the true adjoint electric

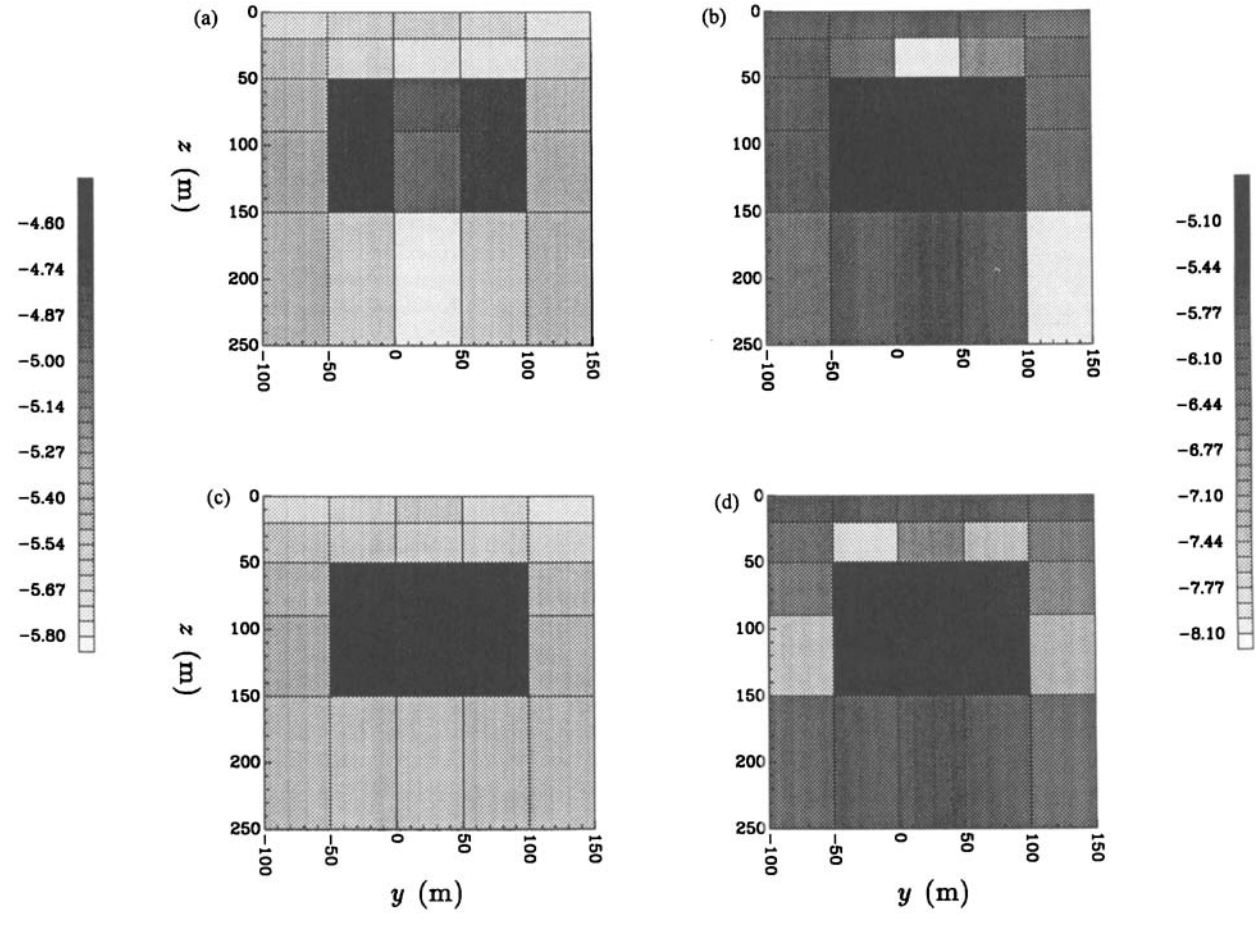

Figure 8. Sensitivities for the 3-D problem described in Section 4.4. The conductivity model comprised a homogeneous background of 0.01 S m^{-1} with a conductive block of 0.1 S m^{-1} coinciding with the cells of enhanced sensitivity shown here. Panels (a) and (c), and the grey-scale on the left of the figure, show $\log_{10}|\partial \ln |H|/\partial \ln \sigma|$, and panels (b) and (d), and the grey-scale on the right of the figure, show $\log_{10}|\partial\phi/\partial \ln \sigma|$. The sensitivities shown are those for the shaded cells in Fig. 6. Panels (a) and (b) were produced by the brute-force method, and panels (c) and (d) were produced by the approximate-sensitivity program using an adjoint field computed in a layered half-space.

field with an approximate adjoint field computed in a uniform or layered half-space. The sensitivities are general and can be used for any source–receiver geometry. We have shown that they are good approximations to the exact sensitivities for 2-, 2.5- and 3-D problems, and that the level of approximation may be sufficiently accurate to enable standard inversion procedures to converge to an acceptable solution. The effectiveness of the approximation depends upon the complexity of structure in the true, multidimensional conductivity model, the closeness of structure to the transmitter and observation locations, and the magnitude of the conductivity contrasts, as well as the particular choice of homogeneous or layered half-space in which the approximate adjoint field is computed. Our exploration of these factors has not been exhaustive, but we are confident that the approximation presented in this paper will prove useful in a large number of situations.

There are clearly other ways to compute an approximate adjoint field, for example by carrying out a partial solution to the full adjoint equation in the true, multidimensional conductivity model. The approximation presented in this paper is, in some ways, rather crude, and yet has enabled inversion procedures to converge to acceptable solutions. One would expect, therefore, that any reasonable approximation to the true adjoint field will produce useful sensitivities. As always, the trade-off between computational requirements and increased accuracy will determine which approximation, if any, is the most desirable.

The approximate sensitivities presented here are significantly faster to compute than the exact sensitivities, by at least an order of magnitude for 2-D problems and two orders of magnitude for 3-D problems. Also, the relative difference in computation times increases as the size of the problem increases. The computation time for the approximate sensitivities is almost independent of the number of observation locations and varies linearly with the number of frequencies and the number of model parameters, whereas that for exact sensitivities would be expected to increase linearly with the number of observation locations and frequencies, and to vary with at least the square of the number of model parameters. The use of these approximate sensitivities will hopefully expand the size of inverse problems that can be tackled on today's computers.

ACKNOWLEDGMENTS

We would like to thank Dr Martyn Unsworth for the use of his 2.5-D forward-modelling and inversion programs, and Dr Art Raiche for the use of SAMAYA. We would also like to thank Drs Rob Ellis and Yaoguo Li for their ever-useful advice, and Dr Greg Newman and an anonymous reviewer for their comments on our manuscript. CGF gratefully acknowledges receipt of a Commonwealth Scholarship. This research was supported by NSERC grant 5-84270.

REFERENCES

Alumbaugh, D.L. & Morrison, H.F., 1995. Theoretical and practical considerations for crosswell electromagnetic tomography assuming a cylindrical geometry, *Geophysics,* **60,** 846–870.

Anderson, W.L., 1979. Numerical integration of related Hankel transforms of orders 0 and 1 by adaptive digital filtering, *Geophysics,* **44,** 1287–1305.

deGroot-Hedlin, C. & Constable, S., 1990. Occam's inversion to generate smooth, two-dimensional models for magnetotelluric data, *Geophysics,* **55,** 1613–1624.

Ellis, R.G., Farquharson, C.G. & Oldenburg, D.W., 1993. Approximate inverse mapping inversion of the COPROD2 Data, *J. Geomag. Geoelectr.,* **45,** 1001–1012.

Gradshteyn, I.S. & Ryzhik, I.M., 1994. *Table of Integrals, Series, and Products,* 5th edn, Academic Press, Boston, MA.

Gupta, P.K., Raiche, A.P. & Sugeng, F., 1989. Three-dimensional time-domain electromagnetic modelling using a compact finite-element frequency-stepping method, *Geophys. J. Int.,* **96,** 457–468.

Hohmann, G.W., 1988. Numerical modeling for electromagnetic methods of geophysics, in *Electromagnetic Methods in Applied Geophysics,* Vol. 1, pp. 313–363, ed. Nabighian, M.N., *Soc. Expl. Geophys.,* Tulsa, OK.

Jupp, D.L.B. & Vozoff, K., 1975. Stable iterative methods for the inversion of geophysical data, *Geophys. J. R. astr. Soc.,* **42,** 957–976.

Kaufman, A.A. & Keller, G.V., 1983. *Frequency and Transient Soundings,* Elsevier, Amsterdam.

Lee, K.H. & Morrison, H.F., 1984. A solution for TM-mode plane waves incident on a two-dimensional inhomogeneity, *Lawrence Berkeley Lab.,* Rep. LBL-17857.

Mackie, R.L. & Madden, T.R., 1993. Three-dimensional magnetotelluric inversion using conjugate gradients, *Geophys. J. Int.,* **115,** 215–229.

Madden, T.R., 1972. Transmission systems and network analogies to geophysical forward and inverse problems, *Tech. Rep.,* **72–3,** Department of Earth and Planetary Sciences, MIT.

Madden, T.R., 1990. Inversion of low frequency electromagnetic data, in *Oceanographic and Geophysical Tomography,* pp. 379–408, eds Desaubies, Y., Tarantola, A. & Vinn-Justin, J., Elsevier, Amsterdam.

Madden, T.R. & Mackie, R.L., 1989. Three-dimensional magnetotelluric modeling and inversion, *Proc. Inst. Electron. Electric. Eng.,* **77,** 318–333.

McGillivray, P.R. & Oldenburg, D.W., 1990. Methods for calculating Fréchet derivatives and sensitivities for the non-linear inverse problem: a comparative study, *Geophys. Prospect.,* **38,** 499–524.

McGillivray, P.R., Oldenburg, D.W., Ellis, R.G. & Habashy, T.M., 1994. Calculation of sensitivities for the frequency-domain electromagnetic problem, *Geophys. J. Int.,* **116,** 1–4.

Newman, G.A., Hohmann, G.W. & Anderson, W.L., 1986. Transient electromagnetic response of a three-dimensional body in a layered earth, *Geophysics,* **51,** 1608–1627.

Oldenburg, D.W. & Ellis, R.G., 1993. Efficient inversion of magnetotelluric data in two dimensions, *Phys. Earth planet. Inter.,* **81,** 177–200.

Oldenburg, D.W., McGillivray, P.R. & Ellis, R.G., 1993. Generalised subspace methods for large scale inverse problems, *Geophys. J. Int.,* **114,** 12–20.

Oristaglio, M.L. & Worthington, M.H., 1980. Inversion of surface and borehole electromagnetic data for two-dimensional electrical conductivity models, *Geophys. Prospect.,* **28,** 633–657.

Park, S.K., 1987. Inversion of magnetotelluric datas for multi-dimensional structure, *Inst. Geophys. planet. Phys.,* **Rep. 87/6,** University of California, San Diego, CA.

Sena, A.G. & Toksöz, M.N., 1990. Simultaneous reconstruction of permittivity and conductivity for crosshole geometries, *Geophysics,* **55,** 1302–1311.

Smith, J.T. & Booker, J.R., 1991. Rapid inversion of two- and three-dimensional magnetotelluric data, *J. geophys. Res.,* **96,** 3905–3922.

Unsworth, M.J. & Oldenburg, D.W., 1995. Subspace inversion of electromagnetic data—application to mid-ocean ridge exploration, *Geophys. J. Int.,* **123,** 161–168.

Unsworth, M.J., Travis, B.J. & Chave, A.D., 1993. Electromagnetic induction by a finite electric dipole source over a 2-D earth, *Geophysics,* **58,** 198–214.

Ward, S.H. & Hohmann, G.W., 1988. Electromagnetic theory for geophysical applications, in *Electromagnetic Methods in Applied Geophysics,* Vol. 1, pp. 131–311, ed. Nabighian, M.N., *Soc. Expl. Geophys.,* Tulsa, OK.

Weidelt, P., 1975. Inversion of two-dimensional conductivity structures, *Phys. Earth planet. Inter.,* **10,** 282–291.

APPENDIX A: SENSITIVITIES FOR A 2-D INVERSE PROBLEM

For a purely 2-D problem, that is, one in which both the conductivity model and the source are invariant in the strike direction, the adjoint field required to calculate the sensitivities becomes the electric field due to a 2-D dipole source. This can be seen as follows. Consider the particular form of eq. (9) for a given measurement and assume that the model and **E** are invariant in the strike direction, which is chosen here as the y-direction. We obtain

$$\frac{\partial F}{\partial \sigma_j} = \int_{-\infty}^{\infty}\int_{-\infty}^{\infty}\int_{-\infty}^{\infty} \mathbf{E}^{\dagger}(x, y, z)\cdot\mathbf{E}(x, z)\psi_j(x, z)\,dx\,dy\,dz \tag{A1}$$

$$= \int_{-\infty}^{\infty}\int_{-\infty}^{\infty} \psi_j(x, z)\mathbf{E}(x, z)\cdot\left\{\int_{-\infty}^{\infty}\tilde{\mathbf{E}}^{\dagger}(x, y, z)\,dy\right\}dx\,dz, \tag{A2}$$

where F represents the component of interest of the electric or magnetic field. Without loss of generality, the adjoint field can be expressed as a 2-D Fourier transform,

$$\mathbf{E}^{\dagger}(x, y, z) = \frac{1}{4\pi^2}\int_{-\infty}^{\infty}\int_{-\infty}^{\infty}\tilde{\mathbf{E}}^{\dagger}(k_x, k_y, z)\exp[i(k_x x + k_y y)]\,dk_x\,dk_y. \tag{A3}$$

If this expression for the adjoint electric field is substituted into eq. (A2), then the integration with respect to y can be carried out, since

$$\frac{1}{2\pi}\int_{-\infty}^{\infty}\exp(ik_y y)\,dy = \delta(k_y). \tag{A4}$$

This reduces the adjoint field to only its zero along-strike wavenumber component,

$$\frac{\partial F}{\partial \sigma_j} = \int_{-\infty}^{\infty}\int_{-\infty}^{\infty} \psi_j(x, z)\mathbf{E}(x, z)\cdot\left\{\frac{1}{2\pi}\int_{-\infty}^{\infty}\tilde{\mathbf{E}}^{\dagger}(k_x, k_y = 0, z)\exp(ik_x x)\,dk_x\right\}dx\,dz. \tag{A5}$$

The term within the braces is the electric field due to a 2-D source, that is, one that is invariant in the strike direction. Eq. (A5) can therefore be rewritten as

$$\frac{\partial F}{\partial \sigma_j} = \int_A \mathbf{E}(x, z)\cdot\mathbf{E}^{\dagger}(x, z)\psi_j(x, z)\,ds, \tag{A6}$$

where the adjoint field, $\mathbf{E}^{\dagger}$, is now due to a 2-D dipole source at the observation location (x_o, z_o). This is the appropriate expression for the sensitivities for a purely 2-D inverse problem.

APPENDIX B: ELECTRIC FIELDS IN A HOMOGENEOUS HALF-SPACE FOR HORIZONTAL 2-D DIPOLE SOURCES

The first form of approximate sensitivities described in Section 4.1 for a purely 2-D inverse problem requires the computation of the electric field generated in a homogeneous half-space by a 2-D dipole source. This electric field is used as the approximate adjoint field. For application to the 2-D magnetotelluric inverse problem, this approximate adjoint field is required for both electric and magnetic dipole sources oriented in both the x- and y-directions on the surface of the conductivity model.

B.1 Electric dipole source

To develop an expression for the electric field generated in a homogeneous half-space by an x- or y-directed 2-D unit electric dipole, we initially follow the derivation of Kaufman & Keller (1983) for the electric field generated by a finite electric dipole.

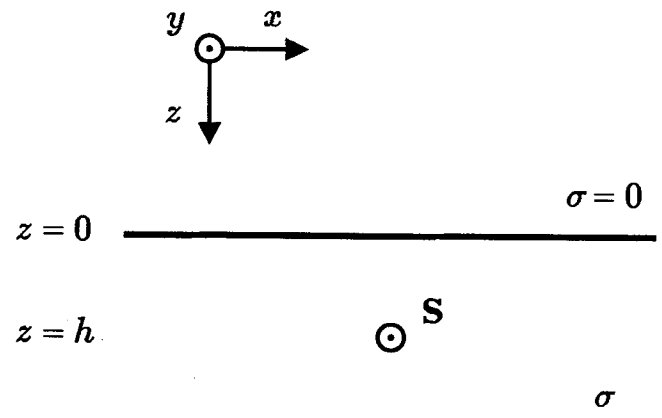

Figure B1. The coordinate system and geometry for computing the electric field induced in a homogeneous half-space by a 2-D dipole source, **S**, using the method described in Appendix B.

Consider an electric dipole oriented in the y-direction and suppose that both the dipole and the point at which the electric field is to be calculated are situated within the conductive half-space (see Fig. B1). Assume that z is positive downwards. Kaufman & Keller make use of the vector potential, $\mathbf{A}$,

$$\mathbf{A} = (0, A_y, A_z), \tag{B1}$$

such that

$$\mathbf{E} = i\omega\mu\mathbf{A} + \frac{1}{\sigma}\nabla(\nabla \cdot \mathbf{A}). \tag{B2}$$

ω is the angular frequency, and μ and σ are the magnetic permeability and conductivity of the half-space. The two non-zero components of the vector potential are

$$A_y = \frac{1}{4\pi}\int_0^\infty \left\{\exp(-u|z-h|) + \frac{u-\lambda}{u+\lambda}\exp[-u(z+h)]\right\}\frac{\lambda}{u}J_0(\lambda\rho)\,d\lambda, \tag{B3}$$

$$A_z = \frac{1}{4\pi}\frac{y}{\rho}\int_0^\infty \frac{2\lambda}{u+\lambda}\exp[-u(z+h)]\,J_1(\lambda\rho)\,d\lambda, \tag{B4}$$

where $u^2 = \lambda^2 + i\omega\mu\sigma$ and $\rho^2 = x^2 + y^2$. We have followed the convention that Ward & Hohmann (1988) use for the time- to frequency-domain Fourier transform. This accounts for the plus sign in the above expression for u. h is the z-coordinate of the dipole source.

Using eq. (2.10) of Ward & Hohmann (1988) to convert the above Hankel transforms to 2-D Fourier transforms gives

$$A_y = \frac{1}{8\pi^2}\int_{-\infty}^\infty\int_{-\infty}^\infty \frac{1}{u}\left\{\exp(-u|z-h|) + \frac{u-\lambda}{u+\lambda}\exp[-u(z+h)]\right\}\exp[i(k_x x + k_y y)]\,dk_x\,dk_y, \tag{B5}$$

$$A_z = -\frac{1}{8\pi^2}\int_{-\infty}^\infty\int_{-\infty}^\infty \frac{2}{\lambda(u+\lambda)}\exp[-u(z+h)]ik_x\exp[i(k_x x + k_y y)]\,dk_x\,dk_y, \tag{B6}$$

where now $\lambda^2 = k_x^2 + k_y^2$. Substituting these two expressions into eq. (B2) gives the three components of the electric field resulting from the y-directed finite electric dipole,

$$E_x = \frac{1}{8\pi^2}\int_{-\infty}^\infty\int_{-\infty}^\infty \left\{\frac{k_x k_y}{\sigma u}\left(\exp(-u|z-h|) + \frac{u-\lambda}{u+\lambda}\exp[-u(z+h)]\right) + \frac{k_x k_y u}{\sigma\lambda(u+\lambda)}\exp[-u(z+h)]\right\}\exp[i(k_x x + k_y y)]\,dk_x\,dk_y, \tag{B7}$$

$$E_y = \frac{1}{8\pi^2}\int_{-\infty}^\infty\int_{-\infty}^\infty \left\{\left(\frac{i\omega\mu}{u} - \frac{k_y^2}{\sigma u}\right)\left(\exp(-u|z-h|) + \frac{u-\lambda}{u+\lambda}\exp[-u(z+h)]\right) - \frac{2k_y^2 u}{\sigma\lambda(u+\lambda)}\exp[-u(z+h)]\right\}\exp[i(k_x x + k_y y)]\,dk_x\,dk_y, \tag{B8}$$

and

$$E_z = -\frac{1}{8\pi^2}\int_{-\infty}^\infty\int_{-\infty}^\infty \left\{\frac{ik_y}{\sigma u}\left(u\,\mathrm{sgn}(z-h)\exp(-u|z-h|) + \frac{u(u-\lambda)}{u+\lambda}\exp[-u(z+h)]\right) + \frac{2ik_y\lambda}{\sigma(u+\lambda)}\exp[-u(z+h)]\right\}\exp[i(k_x x + k_y y)]\,dk_x\,dk_y. \tag{B9}$$

From eq. (A5) we know that the adjoint field required to calculate the sensitivities for a purely 2-D inverse problem can be obtained from the electric field for a finite dipole source by considering only the zero along-strike-wavenumber component. If we do this in the above equations we obtain the following expressions for the electric field generated in a homogeneous half-space by a 2-D y-directed electric dipole source:

$$E_x = 0, \tag{B10}$$

$$E_y = -\frac{i\omega\mu}{2\pi}\int_{-\infty}^{\infty}\frac{1}{u+|k_x|}\exp(-uz)\exp(ik_x x)\,dk_x, \tag{B11}$$

$$E_z = 0, \tag{B12}$$

where it has been assumed that the source is at the surface of the half-space ($h=0$) and now $u^2 = k_x^2 + i\omega\mu\sigma$. From the above equations it is clear that for this type of source there is only an along-strike component of the electric field. This is exactly what is required when calculating the sensitivities for the E-polarization mode of the 2-D magnetotelluric inverse problem. We note that eq. (B11) agrees, as it should, with eq. (4.208) of Ward & Hohmann for the electric field due to an infinite line current.

To obtain expressions for the electric field produced by an x-directed 2-D electric dipole, first consider the electric field produced by a finite x-directed electric dipole. This field is given by eqs (B7) to (B9) after rotation of the coordinate axes corresponding to the transformation $(x, y) \rightarrow (y, -x)$. This implies that $(k_x, k_y) \rightarrow (k_y, -k_x)$ and $(E_x, E_y, E_z) \rightarrow (E_y, -E_x, E_z)$. The electric field due to the 2-D dipole source is then obtained by considering only the components of the equations corresponding to zero along-strike wavenumber,

$$E_x = -\frac{1}{4\pi\sigma}\int_{-\infty}^{\infty} u\{\exp(-u|z-h|) + \exp[-u(z+h)]\}\exp(ik_x x)\,dk_x, \tag{B13}$$

$$E_y = 0, \tag{B14}$$

$$E_z = -\frac{i}{4\pi\sigma}\int_{-\infty}^{\infty} k_x\{\mathrm{sgn}(z-h)\exp(-u|z-h|) + \exp[-u(z+h)]\}\exp(ik_x x)\,dk_x. \tag{B15}$$

The electric field for an x-directed 2-D electric dipole is therefore restricted to lie in the plane perpendicular to the strike direction. The integrals in the above equations can be evaluated (Lee & Morrison 1984) to give analytic expressions for the field components,

$$E_x = -\frac{i\omega\mu}{\pi}\frac{z^2}{r^2}K_0(ikr) + \frac{\omega\mu}{\pi k}\frac{(x^2-z^2)}{r^3}K_1(ikr), \tag{B16}$$

$$E_z = \frac{i\omega\mu}{\pi}\frac{xz}{r^2}K_0(ikr) + \frac{2\omega\mu}{\pi k}\frac{xz}{r^3}K_1(ikr), \tag{B17}$$

where $k^2 = -i\omega\mu\sigma$ and $r^2 = x^2 + z^2$ for the electric dipole on the surface of the half-space. K_0 and K_1 are the zeroth- and first-order modified Bessel functions of the second kind.

B.2 Magnetic dipole source

To develop expressions for the electric field induced in a homogeneous half-space by 2-D magnetic dipole sources we initially follow the analysis of Ward & Hohmann (1988). Consider the Schelkunoff potentials **A** and **F** such that

$$E_x = \frac{1}{\sigma}\frac{\partial^2 A_z}{\partial x \partial z} - \frac{\partial F_z}{\partial y}, \tag{B18}$$

$$E_y = \frac{1}{\sigma}\frac{\partial^2 A_z}{\partial y \partial z} + \frac{\partial F_z}{\partial x}, \tag{B19}$$

$$E_z = \frac{1}{\sigma}\left(\frac{\partial^2}{\partial z^2} + k^2\right)A_z, \tag{B20}$$

where $k^2 = -i\omega\mu\sigma$. For an x-directed magnetic dipole,

$$A_z = \frac{i\omega\mu\sigma}{8\pi^2}\int_{-\infty}^{\infty}\int_{-\infty}^{\infty}\{\exp(-u|z-h|) - \exp[-u(z+h)]\}\frac{ik_y}{u\lambda}\exp[i(k_x x + k_y y)]\,dk_x\,dk_y, \tag{B21}$$

and

$$F_z = -\frac{i\omega\mu}{8\pi^2}\int_{-\infty}^{\infty}\int_{-\infty}^{\infty}\{\exp(-u|z-h|) + \frac{u-\lambda}{u+\lambda}\exp[-u(z+h)]\}\frac{ik_x}{\lambda}\exp[i(k_x x + k_y y)]\,dk_x\,dk_y. \tag{B22}$$

Here, as before, $u^2 = k_x^2 + k_y^2 + i\omega\mu\sigma$ and $\lambda^2 = k_x^2 + k_y^2$. Substituting these expressions into eqs (B18) to (B20) gives

$$E_x = \frac{i\omega\mu}{8\pi^2}\int_{-\infty}^{\infty}\int_{-\infty}^{\infty}\{[\mathrm{sgn}(z-h)-1]\exp(-u|z-h|)+\frac{2\lambda}{u+\lambda}\exp[-u(z+h)]\}\frac{k_x k_y}{\lambda^2}\exp[i(k_x x+k_y y)]\,dk_x\,dk_y, \tag{B23}$$

$$E_y = \frac{i\omega\mu}{8\pi^2}\int_{-\infty}^{\infty}\int_{-\infty}^{\infty}\left(\frac{k_y^2}{\lambda^2}\{\mathrm{sgn}(z-h)\exp(-u|z-h|)+\exp[-u(z+h)]\}\right.$$
$$\left.+\frac{k_x^2}{\lambda^2}\{\exp(-u|z-h|)+\frac{u-\lambda}{u+\lambda}\exp[-u(z+h)]\}\right)\exp[i(k_x x+k_y y)]\,dk_x\,dk_y, \tag{B24}$$

and

$$E_z = \frac{i\omega\mu}{8\pi^2}\int_{-\infty}^{\infty}\int_{-\infty}^{\infty}\frac{ik_y}{u}\{\exp(-u|z-h|)-\exp[-u(z+h)]\}\exp[i(k_x x+k_y y)]\,dk_x\,dk_y. \tag{B25}$$

To obtain expressions for the electric field generated by a 2-D x-directed magnetic dipole on the surface of the half-space, consider the reduced forms of the above equations for $k_y = 0$,

$$E_x = 0, \tag{B26}$$

$$E_y = \frac{i\omega\mu}{2\pi}\int_{-\infty}^{\infty}\frac{u}{u+|k_x|}\exp(-uz)\exp(ik_x x)\,dk_z, \tag{B27}$$

$$E_z = 0. \tag{B28}$$

For a y-directed 2-D magnetic dipole use the transformation $(x, y) \rightarrow (y, -x)$ in eqs (B23) to (B25) before considering the reduced form of these equations. This gives

$$E_x = \frac{i\omega\mu}{2\pi}\int_{-\infty}^{\infty}\exp(-uz)\exp(ik_x x)\,dk_x, \tag{B29}$$

$$E_y = 0, \tag{B30}$$

$$E_z = 0. \tag{B31}$$

Using eq. (3.914) of Gradshteyn & Ryzhik (1994), eq. (B29) can be reduced to

$$E_x = -\frac{\omega\mu k}{\pi}\frac{z}{r}K_1(ikr), \tag{B32}$$

where $k^2 = -i\omega\mu\sigma$ and $r^2 = x^2 + z^2$.

The electric fields described above were computed by evaluation of the Bessel functions or, if the expression for the electric field could not be reduced to one involving Bessel functions, by evaluation of the Fourier transform using the digital filtering code of Newman, Hohmann & Anderson (1986).

APPENDIX C: FIELDS IN A HORIZONTALLY LAYERED HALF-SPACE FOR HORIZONTAL DIPOLE SOURCES

We outline here the method that we used to calculate the electric field induced in a horizontally layered half-space by a dipole source. We consider horizontal electric and magnetic dipole sources that can either be point sources in 3-D space or, if only the zero along-strike-wavenumber component of the field is considered, in 2-D space. The layered half-space comprises layers of constant conductivity, as shown in Fig. C1. We use the TE and TM mode Schelkunoff potentials of Ward & Hohmann (1988),

$$\mathbf{A} = A\hat{\mathbf{e}}_z, \tag{C1}$$

$$\mathbf{F} = F\hat{\mathbf{e}}_z. \tag{C2}$$

In the jth layer, A and F satisfy the following ordinary differential equations:

$$\left(\frac{d^2}{dz^2} - u_j^2\right)\tilde{A}_j = 0, \tag{C3}$$

$$\left(\frac{d^2}{dz^2} - u_j^2\right)\tilde{F}_j = 0, \tag{C4}$$

where the tilde represents the 2-D Fourier transform, $u_j^2 = k_x^2 + k_y^2 + i\omega\mu\sigma_j - \mu\varepsilon\omega^2$, ω is the angular frequency, μ is the magnetic

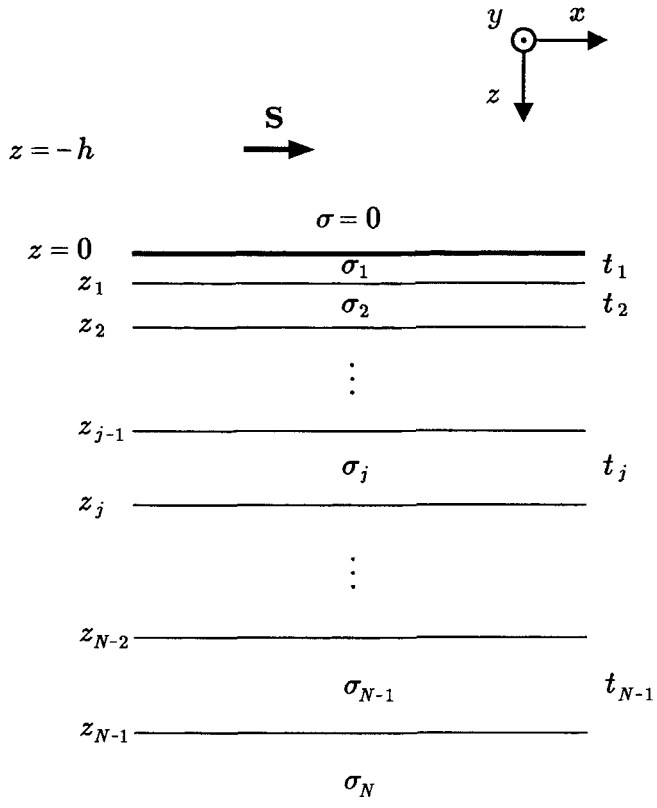

Figure C1. The coordinate system, geometry and notation used in computing the electric field in a layered half-space by the method described in Appendix C. **S** represents the dipole source.

permeability and σ_j is the conductivity of the jth layer. The solutions for $\tilde{A}_j$ and $\tilde{F}_j$ are

$$\tilde{A}_j(k_x, k_y, z, \omega) = C_j(k_x, k_y, \omega)\exp[u_j(z - z_{j-1})] + D_j(k_x, k_y, \omega)\exp[-u_j(z - z_{j-1})], \tag{C5}$$

$$\tilde{F}_j(k_x, k_y, z, \omega) = U_j(k_x, k_y, \omega)\exp[u_j(z - z_{j-1})] + V_j(k_x, k_y, \omega)\exp[-u_j(z - z_{j-1})]. \tag{C6}$$

In the region of free space above the layered half-space, let

$$\tilde{A}_0 = C_0\exp(u_0 z) + D_0\exp(-u_0 z) \tag{C7}$$

$$\tilde{F}_0 = U_0\exp(u_0 z) + V_0\exp(-u_0 z), \tag{C8}$$

where $u_0^2 = k_x^2 + k_y^2$.

First, consider the potential F. From Ward & Hohmann eqs (1.174) and (1.175), the boundary conditions on $\tilde{F}$ at $z = z_{j-1}$ are

$$\tilde{F}_j(k_x, k_y, z = z_{j-1}, \omega) = \tilde{F}_{j-1}(k_x, k_y, z = z_{j-1}, \omega), \tag{C9}$$

$$\frac{\partial \tilde{F}_j}{\partial z}(k_x, k_y, z = z_{j-1}, \omega) = \frac{\partial \tilde{F}_{j-1}}{\partial z}(k_x, k_y, z = z_{j-1}, \omega). \tag{C10}$$

Substituting eq. (C6) into the above boundary conditions gives

$$U_j + V_j = U_{j-1}\exp(u_{j-1}t_{j-1}) + V_{j-1}\exp(-u_{j-1}t_{j-1}), \tag{C11}$$

$$u_j U_j - u_j V_j = u_{j-1}U_{j-1}\exp(u_{j-1}t_{j-1}) - u_{j-1}V_{j-1}\exp(-u_{j-1}t_{j-1}). \tag{C12}$$

$t_j = z_j - z_{j-1}$ is the thickness of the jth layer. These two boundary conditions can be combined in a matrix equation,

$$\begin{pmatrix} 1 & 1 \\ u_j & -u_j \end{pmatrix}\begin{pmatrix} U_j \\ V_j \end{pmatrix} = \begin{pmatrix} \exp(u_{j-1}t_{j-1}) & \exp(-u_{j-1}t_{j-1}) \\ u_{j-1}\exp(u_{j-1}t_{j-1}) & -u_{j-1}\exp(-u_{j-1}t_{j-1}) \end{pmatrix}\begin{pmatrix} U_{j-1} \\ V_{j-1} \end{pmatrix}. \tag{C13}$$

This can be rewritten as

$$\begin{pmatrix} U_{j-1} \\ V_{j-1} \end{pmatrix} = \frac{1}{2}\exp(u_{j-1}t_{j-1})\mathbf{M}_j\begin{pmatrix} U_j \\ V_j \end{pmatrix}, \tag{C14}$$

where

$$\mathbf{M}_j = \begin{pmatrix} \left(1+\frac{u_j}{u_{j-1}}\right)\exp(-2u_{j-1}t_{j-1}) & \left(1-\frac{u_j}{u_{j-1}}\right)\exp(-2u_{j-1}t_{j-1}) \\ \left(1-\frac{u_j}{u_{j-1}}\right) & \left(1+\frac{u_j}{u_{j-1}}\right) \end{pmatrix}. \tag{C15}$$

In eq. (C14), the exponential term $\exp(u_{j-1}t_{j-1})$ has been factored out of the matrix $\mathbf{M}_j$ so that the propagation through the layers carried out below remains stable. Applying the boundary conditions at the surface of the half-space and using eq. (C8) for the potential $\tilde{F}$ in the free space above the layered half-space leads to

$$\begin{pmatrix} U_0 \\ V_0 \end{pmatrix} = \frac{1}{2}\mathbf{M}_1 \begin{pmatrix} U_1 \\ V_1 \end{pmatrix}, \tag{C16}$$

where

$$\mathbf{M}_1 = \begin{pmatrix} \left(1+\frac{u_1}{u_0}\right) & \left(1-\frac{u_1}{u_0}\right) \\ \left(1-\frac{u_1}{u_0}\right) & \left(1+\frac{u_1}{u_0}\right) \end{pmatrix}. \tag{C17}$$

Eqs (C16) and (C14) can be used to propagate the boundary conditions through the layers to produce an expression relating the coefficients of the potential $\tilde{F}$ in the free space above the half-space to those in the basement half-space,

$$\begin{pmatrix} U_0 \\ V_0 \end{pmatrix} = \left(\frac{1}{2}\right)^{N+1} \exp\left(\sum_{j=1}^{N} u_j t_j\right) \prod_{j=1}^{N+1} \mathbf{M}_j \begin{pmatrix} U_{N+1} \\ V_{N+1} \end{pmatrix}. \tag{C18}$$

There can be no upward-decaying solution for $\tilde{F}$ in the basement half-space, so $U_{N+1} = 0$. It is assumed that the source is at a height $z = -h$ above the layered half-space. If this source is an x-directed electric dipole then, from eq. (4.137) of Ward & Hohmann,

$$V_0 = \frac{\omega\mu}{2u_0}\frac{k_y}{k_x^2+k_y^2}\exp(-u_0 h). \tag{C19}$$

For an x-directed magnetic dipole,

$$V_0 = \frac{\omega\mu}{2}\frac{k_x}{k_x^2+k_y^2}\exp(-u_0 h), \tag{C20}$$

using eq. (4.106) of Ward & Hohmann. Eq. (C18) is therefore a pair of simultaneous equations in the two unknowns U_0 and V_{N+1}. Once U_0 is known, eq. (C16) can be used to obtain U_1 and V_1. Successive applications of eq. (C14) then give the coefficients U_j and V_j, and hence the potential $\tilde{F}$, in every layer.

A modified version of the above approach was used for the potential $\tilde{A}$. The boundary conditions on $\tilde{A}$ at $z = z_{j-1}$ are, from Ward & Hohmann eqs (1.182) and (1.183),

$$\tilde{A}_j(k_x, k_y, z = z_{j-1}, \omega) = \tilde{A}_{j-1}(k_x, k_y, z = z_{j-1}, \omega), \tag{C21}$$

$$\frac{1}{\sigma_j + i\varepsilon\omega}\frac{\partial \tilde{A}_j}{\partial z}(k_x, k_y, z = z_{j-1}, \omega) = \frac{1}{\sigma_{j-1} + i\varepsilon\omega}\frac{\partial \tilde{A}_{j-1}}{\partial z}(k_x, k_y, z = z_{j-1}, \omega). \tag{C22}$$

Because of the awkwardness, numerically, of the second boundary condition at the surface of the layered half-space (above which $\sigma = 0$), the source is assumed to lie within layer 1 (at $z = h$). The final result for the source on the surface of the half-space is obtained by letting the source approach the surface from below. In layer 1, therefore, eq. (C5) is modified to contain a term representing the particular solution,

$$\tilde{A}_1 = C_1 \exp(u_1 z) + D_1 \exp(-u_1 z) + \tilde{A}_p \exp(-u_1|z-h|). \tag{C23}$$

Extending the analysis of Ward & Hohmann to determine explicit expressions for their quantity A_p, the appropriate expression for $\tilde{A}_p$, in eq. (C23) for a unit x-directed electric dipole is

$$\tilde{A}_p = -\frac{1}{2}\frac{ik_x}{k_x^2+k_y^2}, \tag{C24}$$

and

$$\tilde{A}_p = -\frac{\mu\varepsilon\omega^2 - i\omega\mu\sigma_1}{2u_1}\frac{ik_y}{k_x^2 + k_y^2} \tag{C25}$$

for a unit x-directed magnetic dipole. The boundary conditions can now be propagated through the layers in a similar manner to the potential $\tilde{F}$ to obtain two simultaneous equations in the two unknowns C_0 and D_{N+1} (D_0 is zero since there is now no downward-decaying part of the solution in the free space above the half-space). To obtain the potentials for y-directed electric and magnetic dipoles, the transformation $(x, y) \rightarrow (y, -x)$ $[\Rightarrow (k_x, k_y) \rightarrow (k_y, -k_x)]$ can be used.

Once the potentials $\tilde{A}$ and $\tilde{F}$ are known, the components of the electric and magnetic fields can be calculated throughout the layered half-space using eqs (1.129) and (1.130) of Ward & Hohmann,

$$E_x = \frac{1}{\sigma + i\varepsilon\omega}\frac{\partial^2 A}{\partial x \partial z} - \frac{\partial F}{\partial y}, \tag{C26}$$

$$E_y = \frac{1}{\sigma + i\varepsilon\omega}\frac{\partial^2 A}{\partial y \partial z} + \frac{\partial F}{\partial x}, \tag{C27}$$

$$E_z = \frac{1}{\sigma + i\varepsilon\omega}\left(\frac{\partial^2}{\partial z^2} + k^2\right)A, \tag{C28}$$

and

$$H_x = \frac{\partial a}{\partial y} + \frac{1}{i\omega\mu}\frac{\partial^2 F}{\partial x \partial z}, \tag{C29}$$

$$H_y = -\frac{\partial A}{\partial x} + \frac{1}{i\omega\mu}\frac{\partial^2 F}{\partial y \partial z}, \tag{C30}$$

$$H_z = \frac{1}{i\omega\mu}\left(\frac{\partial^2}{\partial z^2} + k^2\right)F, \tag{C31}$$

where $k^2 = \mu\varepsilon\omega^2 - i\omega\mu\sigma$. The above equations are in fact transformed to the (k_x, k_y) domain and used to obtain $\tilde{E}$ and $\tilde{H}$ from $\tilde{A}$ and $\tilde{F}$, and then the transformation back to the (x, y) domain that is appropriate for the particular problem is carried out. For the purely 2-D case discussed in Section 4.1, the electric field for the appropriate 2-D dipole source can be obtained by setting the along-strike wavenumber, k_y, equal to zero. For the 2.5-D case discussed in Section 4.3, the inverse cosine/sine transform with respect to the across-strike wavenumber, k_x, is performed on the electric field. The scalar product of this field with the electric field, **E**, from the forward modelling is then calculated while still in the along-strike-wavenumber (k_y) domain before this remaining wavenumber dependence is integrated out to produce the desired sensitivity. Finally, for the 3-D case described in Section 4.4, the 2-D Fourier transform with respect to k_x and k_y is converted to a Hankel transform using eq. (2.10) of Ward & Hohmann. The cosine/sine transforms were evaluated using the method of Newman *et al.* (1986), and the Hankel transform was evaluated using the method of Anderson (1979).

APPENDIX D: SENSITIVITIES FOR THE MAGNETOTELLURIC APPARENT RESISTIVITY AND PHASE

In the magnetotelluric inverse problem, the data are usually considered to be values of the apparent resistivity, ρ_a, and phase, ϕ, where

$$\rho_a(\omega) = \frac{1}{\omega\mu}\left|\frac{E}{H}\right|^2 \quad \text{and} \quad \phi(\omega) = \text{phase}\left(\frac{E}{H}\right). \tag{D1}$$

E and H represent orthogonal horizontal components of the electric and magnetic fields. Since it is the apparent resistivity and phase that are the data in the inverse problem, the sensitivities are required for these data rather than for the electric and magnetic fields. However, the sensitivities for the apparent resistivity and phase can be obtained from those for the electric and magnetic fields as follows. Differentiating the apparent resistivity in eq. (D1) with respect to the model parameter σ_j gives

$$\frac{\partial \rho_a}{\partial \sigma_j} = \frac{2}{\omega\mu}\left|\frac{E}{H}\right|\frac{\partial}{\partial \sigma_j}\left(\frac{|E|}{|H|}\right) \tag{D2}$$

$$= \frac{2}{\omega\mu}\left|\frac{E}{H}\right|\left\{\frac{1}{|H|}\frac{\partial |E|}{\partial \sigma_j} - \frac{|E|}{|H|^2}\frac{\partial |H|}{\partial \sigma_j}\right\}. \tag{D3}$$

Since the electric field in the frequency domain is a complex quantity it can be written as

$$E = |E| \exp(i\Phi_E). \tag{D4}$$

Treating both $|E|$ and Φ_E as functions of the model parameters, differentiating eq. (D4) with respect to σ_j gives

$$\frac{\partial E}{\partial \sigma_j} = |E| \frac{\partial}{\partial \sigma_j} [\exp(i\Phi_E)] + \frac{\partial |E|}{\partial \sigma_j} \exp(i\Phi_E) \tag{D5}$$

$$= i|E| \exp(i\Phi_E) \frac{\partial \Phi_E}{\partial \sigma_j} + \frac{E}{|E|} \frac{\partial |E|}{\partial \sigma_j} \tag{D6}$$

$$\Rightarrow \frac{1}{E} \frac{\partial E}{\partial \sigma_j} = i \frac{\partial \Phi_E}{\partial \sigma_j} + \frac{1}{|E|} \frac{\partial |E|}{\partial \sigma_j}. \tag{D7}$$

Equating the real and imaginary parts of eq. (D7) gives

$$\frac{\partial |E|}{\partial \sigma_j} = |E| \, \mathcal{R}e\left(\frac{1}{E} \frac{\partial E}{\partial \sigma_j} \right) \tag{D8}$$

and

$$\frac{\partial \Phi_E}{\partial \sigma_j} = \mathcal{I}m\left(\frac{1}{E} \frac{\partial E}{\partial \sigma_j} \right). \tag{D9}$$

This argument can also be applied to the magnetic field, resulting in

$$\frac{\partial |H|}{\partial \sigma_j} = |H| \, \mathcal{R}e\left(\frac{1}{H} \frac{\partial H}{\partial \sigma_j} \right) \tag{D10}$$

and

$$\frac{\partial \Phi_H}{\partial \sigma_j} = \mathcal{I}m\left(\frac{1}{H} \frac{\partial H}{\partial \sigma_j} \right). \tag{D11}$$

Eqs (D8) and (D10) can be substituted into eq. (D3) to give a final expression for the sensitivity of the apparent resistivity,

$$\frac{\partial \rho_a}{\partial \sigma_j} = \frac{2}{\omega \mu} \left| \frac{E}{H} \right| \left\{ \frac{|E|}{|E|} \mathcal{R}e\left(\frac{1}{E} \frac{\partial E}{\partial \sigma_j} \right) - \frac{|E|}{|H|} \mathcal{R}e\left(\frac{1}{H} \frac{\partial H}{\partial \sigma_j} \right) \right\} \tag{D12}$$

$$= 2\rho_a \left\{ \mathcal{R}e\left(\frac{1}{E} \frac{\partial E}{\partial \sigma_j} \right) - \mathcal{R}e\left(\frac{1}{H} \frac{\partial H}{\partial \sigma_j} \right) \right\}. \tag{D13}$$

This expression can be used to calculate the sensitivity of the apparent resistivity since ρ_a is known at the observation location and $\partial E/\partial \sigma_j$ and $\partial H/\partial \sigma_j$ can be calculated using the formula given at the end of Section 2 (see eq. 9).

To determine the final expression for the sensitivity of the phase, consider the ratio

$$\frac{E}{H} = \frac{|E| \exp(i\Phi_E)}{|H| \exp(i\Phi_H)} = \left| \frac{E}{H} \right| \exp[i(\Phi_E - \Phi_H)]. \tag{D14}$$

By definition,

$$\phi = \Phi_E - \Phi_H, \tag{D15}$$

so

$$\frac{\partial \phi}{\partial \sigma_j} = \frac{\partial \Phi_E}{\partial \sigma_j} - \frac{\partial \Phi_H}{\partial \sigma_j} \tag{D16}$$

$$= \mathcal{I}m\left(\frac{1}{E} \frac{\partial E}{\partial \sigma_j} \right) - \mathcal{I}m\left(\frac{1}{H} \frac{\partial H}{\partial \sigma_j} \right), \tag{D17}$$

using eqs (D9) and (D11). The sensitivity in the phase can therefore be calculated using eq. (D17) and the formula at the end of Section 2.